

# Silencing of the *Drosophila* ortholog of SOX5 in heart leads to cardiac dysfunction as detected by optical coherence tomography

Airong Li<sup>1,†</sup>, Osman O. Ahsen<sup>4,†</sup>, Jonathan J. Liu<sup>4</sup>, Chuang Du<sup>5</sup>, Mary L. McKee<sup>2</sup>, Yan Yang<sup>1</sup>, Wilma Wasco<sup>1</sup>, Christopher H. Newton-Cheh<sup>3</sup>, Christopher J. O'Donnell<sup>6</sup>, James G. Fujimoto<sup>4</sup>, Chao Zhou<sup>4,7,\*</sup> and Rudolph E. Tanzi<sup>1,\*</sup>

<sup>1</sup>Genetics and Aging Research Unit, Department of Neurology, MassGeneral Institute for Neurodegenerative Diseases, <sup>2</sup>Program in Membrane Biology and <sup>3</sup>Department of Medicine, Massachusetts General Hospital and Harvard Medical School, Charlestown, MA, USA, <sup>4</sup>Department of Electrical Engineering and Computer Science, Research Laboratory of Electronics, Massachusetts Institute of Technology, Cambridge, MA, USA, <sup>5</sup>Center for Neuroscience Research, Tufts University School of Medicine, Boston, MA, USA, <sup>6</sup>Framingham Heart Study, The National Heart, Lung, and Blood Institute (NHLBI), Framingham, MA, USA and <sup>7</sup>Department of Electrical and Computer and Engineering, Lehigh University, Bethlehem, PA, USA

Received January 24, 2013; Revised and Accepted May 16, 2013

Downloaded from <http://hmg.oxfordjournals.org/> at Lehigh University on June 7, 2013

The SRY-related HMG-box 5 (*SOX5*) gene encodes a member of the SOX family of transcription factors. Recently, genome-wide association studies have implicated *SOX5* as a candidate gene for susceptibility to four cardiac-related endophenotypes: higher resting heart rate (HR), the electrocardiographic PR interval, atrial fibrillation and left ventricular mass. We have determined that human *SOX5* has a highly conserved *Drosophila* ortholog, *Sox102F*, and have employed transgenic *Drosophila* models to quantitatively measure cardiac function in adult flies. For this purpose, we have developed a high-speed and ultrahigh-resolution optical coherence tomography imaging system, which enables rapid cross-sectional imaging of the heart tube over various cardiac cycles for the measurement of cardiac structural and dynamical parameters such as HR, dimensions and areas of heart chambers, cardiac wall thickness and wall velocities. We have found that the silencing of *Sox102F* resulted in a significant decrease in HR, heart chamber size and cardiac wall velocities, and a significant increase in cardiac wall thickness that was accompanied by disrupted myofibril structure in adult flies. In addition, the silencing of *Sox102F* in the wing led to increased L2, L3 and wing marginal veins and increased and disorganized expression of wingless, the central component of the Wnt signaling pathway. Collectively, the silencing of *Sox102F* resulted in severe cardiac dysfunction and structural defects with disrupted Wnt signaling transduction in flies. This implicates an important functional role for *SOX5* in heart and suggests that the alterations in *SOX5* levels may contribute to the pathogenesis of multiple cardiac diseases or traits.

## INTRODUCTION

The SRY-related HMG-box 5 (*SOX5*) gene is localized on chromosome 12p12 (OMIM 604975) and encodes a member of the SOX family of transcription factors that bind to DNA (1).

*SOX5* is expressed in multiple human tissues, including heart, liver, lung, kidney, spleen, fetal brain and testis (2). Studies have shown that *SOX5* can modulate cell fate, control cell proliferation and regulate cartilage formation and neuron

\*To whom correspondence should be addressed at: Genetics and Aging Research Unit, Department of Neurology, Massachusetts General Hospital, 114, 16th Street, Charlestown, MA 02129, USA. Tel: +1 6177266845; Fax: +1 6177241949; Email: tanzi@helix.mgh.harvard.edu (R.E.T.); Department of Electrical and Computer and Engineering, Lehigh University, 19 Memorial Drive West, Bethlehem, PA 18015-3084, USA. Tel: +1 6107585092; Fax: +1 6107586279; Email: chaozhou@lehigh.edu (C.Z.)

†These authors contributed equally.

development (3–5). Recently, genome-wide association studies (GWASs) have implicated SOX5 as a candidate gene for susceptibility to four cardiac-related endophenotypes: higher resting heart rate (RHR) (6), the electrocardiographic PR interval (7), atrial fibrillation (AF) (8) and left ventricular mass (LVM) (9). These findings suggest an important functional role for SOX5 in the heart. Mice with *Sox5* gene single null mutation were early lethal and had mild skeletal abnormalities (3). *Sox5*-deficient mice died at birth with respiratory distress and abnormal lung development, indicating that *Sox5* is critical for proper *in utero* lung morphogenesis (10). To date, early lethality in loss of function *Sox5* mouse models has prohibited analysis of adult cardiac function; a role for SOX5 in cardiac function has not been reported previously.

*Drosophila melanogaster* or fruit fly has been successfully used to characterize multiple genes associated with cardiac diseases (11–14). The basic mechanisms of heart development and control of cardiac function are highly conserved between human and *Drosophila*. Thus, discoveries made in the fly can be applied to higher species including human. In addition, *Drosophila* have a short life span and an oxygen transport system independent from its heart, which makes the organism more viable to genetic alterations that effect cardiac function (15). Anatomically, the fly heart lies close to the dorsal surface of the abdomen (14). Therefore, the morphological and rhythm changes can be readily analyzed in the relatively simple organization of the fly heart with the emerging biomedical imaging technology optical coherence tomography (OCT) (16).

Non-invasive OCT enables real-time, *in vivo*, micron-scale and three-dimensional (3D) imaging of biological tissues without the need to sacrifice and process specimens. OCT has been used for a wide range of clinical applications in human, including ophthalmology (16–19), endoscopy (20–26) and cardiovascular imaging (27–31). *Drosophila*'s heart beats at a rate of several hundred beats per minute (BPM), making high imaging speed critical in order to capture the dynamics of its heart during various cardiac cycles. The utility of OCT for studying *Drosophila* cardiac functions has been reported by several studies (32–37). With a custom-built OCT imaging platform, we previously demonstrated acquiring cross-sectional OCT images at ~120 frames/s, fast enough to capture the dynamics of the beating *Drosophila* heart, in order to assess the effect of Alzheimer's disease and dilated cardiomyopathy-associated presenilin gene. We found that either the overexpression or the silencing of the *Drosophila* ortholog of presenilin in the heart leads to cardiac dysfunction (36). To date, OCT has been used by our group and others to evaluate cardiac function using M-mode imaging at a single location of the *Drosophila* heart tube over time and concentrated on inferring structural information, such as heart dimensions during systole and diastole phase, as well as functional information, such as HR and arrhythmia prevalence, and to detect significant differences in these cardiac parameters in response to genetic alterations related to cardiac diseases (32–34,36). Previous studies, however, lacked the resolution and speed to resolve fine details such as cardiac wall dimensions, as well as the ability to measure wall dynamics using information from the entire cross-sectional heart chamber (32–34,36). With the advancements in the imaging speed as well as Doppler and phase sensitive detection, the use of OCT for *Drosophila* studies was further extended to

study the dynamics of cardiac wall movement during various cardiac cycles (35,37).

In this study, we have developed a high-speed and ultrahigh-resolution OCT imaging system to non-invasively quantify *Drosophila* cardiac function more precisely and more comprehensively than previously possible. The new OCT system enables the 3D volumetric imaging of the *Drosophila* and rapidly captures the cross-sectional images of the heart tube over various cardiac cycles. By searching the *Drosophila* genome database, we determined that human SOX5 is highly conserved to a *Drosophila* ortholog *Sox102F*. *SOX5* and *Sox102F* share 71% identity and 82% similarity in amino acid sequences. To circumvent the lethality of mouse models null for *Sox5*, we have employed transgenic *Drosophila* models and high-performance OCT imaging to quantitatively measure cardiac function in adult flies to assess the functional role of *Sox102F* in the heart. Our studies have demonstrated that the silencing of *Sox102F* in the heart results in cardiac dysfunction.

## RESULTS

### *Drosophila* cardiac function and heart structural analysis

We employed UAS-*Sox102F*-RNAi transgenic flies and an established 24B-GAL4 driver (38) to silence *Sox102F* specifically in the fly heart (38,39). The 24B-GAL4 line allows targeted expression in mesoderm and all cardiac and muscular cells with a uniform and high level of expression in the most anterior heart cells (40). Flies in which *Sox102F* was silenced by 24B-GAL4 (UAS-*Sox102F*-RNAi; 24B-GAL4) appeared normal at eclosion. The silencing of *Sox102F* led to a decrease in *Sox102F* expression to 55% compared with control flies that expressed a heterozygous 24B-GAL4 alone (24B-GAL4/+), as assessed by real-time reverse transcriptase (RT)-polymerase chain reaction (PCR) of cDNA from the hearts of the UAS-*Sox102F*-RNAi; 24B-GAL4 and 24B-GAL4/+ flies.

We quantitatively measured cardiac function in 30-day-old UAS-*Sox102F*-RNAi; 24B-GAL4 flies ( $n = 35$ ) and age-matched control flies ( $n = 36$ ) using the newly developed OCT system. Since the imaging resolution and speed were dramatically improved compared with our previous system (36), this analysis allows us to have a more precise measurement of the chamber dimensions, as well as enables us to use Doppler OCT to measure cardiac wall velocity versus time. As can be seen in Figure 1, where an example of volumetric and cross-sectional OCT images of an adult *Drosophila* are shown, OCT can readily identify at least the first three heart segments (ostia) of the fly (Fig. 1B).

Analyses of OCT imaging data for assessing cardiac function were categorized as structural parameters, including the end systolic and diastolic vertical and transverse dimensions (ESDv, ESDt, EDDv and EDDt), end systolic and diastolic areas (ESA and EDA) and cardiac wall thickness and dynamical parameters, including HR, systolic and diastolic wall velocities and the prevalence of arrhythmia (Table 1). Compared with the age-matched controls, structurally, the silencing of *Sox102F* in flies (UAS-*Sox102F*-RNAi; 24B-GAL4) resulted in a significant decrease in each of the structural parameters, including ESDv, ESDt, EDDv, EDDt, ESA and EDA, and a significant increase in cardiac wall thickness from  $10.80 \pm 0.28 \mu\text{m}$  in

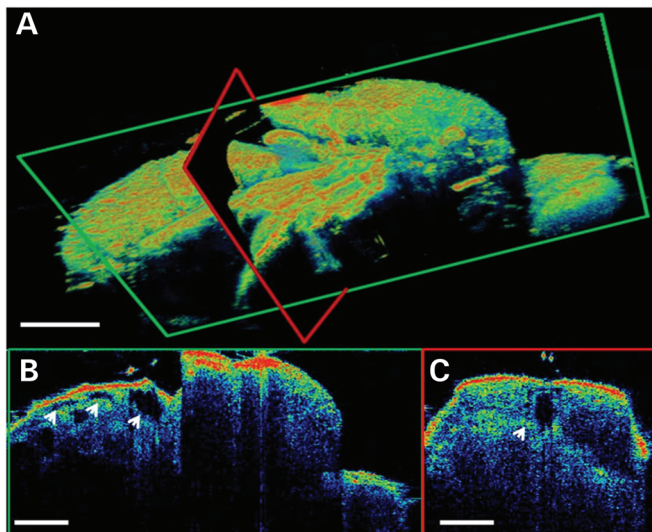


**Figure 1.** OCT imaging of adult *Drosophila*. (A) 3D reconstruction from a volumetric data set of an adult *Drosophila*. (B) Cross-sectional OCT view along the fly body showing detailed structures in the sagittal plane. Arrows point to the first three ostia, identified as empty, elongated tubes. (C) Cross-sectional OCT view across the fly's abdomen showing a detailed structure of the main heart chamber (conical heart chamber). As indicated by the arrow, the heart is observed as an empty space in the images. Images are false color coded and the higher intensity signal is represented by a color closer to red. Scale bars: 250  $\mu$ m.

control to  $12.23 \pm 0.30$   $\mu$ m in UAS-*Sox102F*-RNAi; 24B-GAL4 flies (Table 1, Fig. 2). Dynamically, the silencing of *Sox102F* caused a significant decrease in HR from  $239 \pm 8$  to  $211 \pm 10$  BPM in UAS-*Sox102F*-RNAi flies and both systolic and diastolic wall velocities (Table 1, Figs 2 and 3) and an increase in the cardiac arrhythmia prevalence, although arrhythmia prevalence did not reach statistical significance (Table 1).

We analyzed 30-day-old flies' whole heart by F-actin immunostaining and heart ultrastructure by transmission electron microscopy (TEM). Fluorescent labeling of the whole adult heart with F-actin demonstrated that the silencing of *Sox102F* resulted in an enlarged and irregular cardiac tube and loss of myofibril structure (Fig. 4B) compared with that of control (Fig. 4A). TEM analysis of the adult hearts of control flies showed normal myofibril structure (Fig. 4C and D). In contrast, hearts from flies in which *Sox102F* was silenced revealed irregular and broken myofilament arrays with larger gaps between the individual filaments, discontinuous Z discs, irregular and smaller sarcoplasmic reticulum (SR) and degenerative mitochondria (Fig. 4E and F) consistent with whole heart and cardiac functional alterations. Collectively, these data demonstrate that the silencing of *Sox102F* led to cardiac hypertrophy, a decrease in the size of the heart chamber and a decrease in HR and wall velocities, accompanied by disrupted myofibril structure in adult flies.

### Wing phenotype and wingless expression

Wing development is regulated by multiple signaling pathways, including Notch, Wnt, epidermal growth factor receptor, hedgehog and decapentaplegic. The wing pattern has provided an important tool in isolating and characterizing genes affecting these signaling pathways (41). Wnts are a family of secreted signaling

proteins including wingless (wg), the central component of Wnt signaling pathway (42). To identify the functional pathway of SOX5, we silenced *Sox102F* specifically in the wing. SD-GAL4 drives the silencing of *Sox102F* in the wing disc in the pattern of the *scalloped* (*sd*) gene, which regulates the expression of a number of targeted genes including *wg* (42). Over 200 flies were analyzed for the wing phenotype. Heterozygous SD-GAL4 driver alone (SD-GAL4/+) showed normal wing (Fig. 5A–C). The silencing of *Sox102F* in the wing (UAS-*Sox102F*-RNAi; SD-GAL4) resulted in a significant increase in the L2, L3 and wing marginal veins; in particular, extra veins were formed in the distal part of L3 (Fig. 5D–F). We next examined the expression of the *wg* protein by immunostaining wing imaginal discs dissected from the third instar larvae with an anti-*wg* antibody. In control flies with heterozygous SD-GAL4 driver alone (SD-GAL4/+), *wg* was expressed as a broad strip in the notum, a thinner strip in the prospective wing margin-dorsal/ventral (D/V) boundary and a strip encircling the prospective wing blade (Fig. 5G). Consistent with the phenotype observed in adult flies, we observed remarkably increased *wg* expression levels and disorganized *wg* expression pattern in the third instar wing discs in which *Sox102F* was silenced, leading to extra strips in the prospective wing blade region (Fig. 5H). These data strongly support *Sox102F* as a regulator of *wg* expression.

### DISCUSSION

In this study, we have provided clear evidence indicating that the silencing of *Sox102F* leads to severe cardiac dysfunction and structural defects in adult flies, including cardiac hypertrophy, reduced heart chamber size and decrease HR and wall velocities, accompanied by disrupted myofibril structure, and that the expression of *Sox102F* can regulate *wg* expression. Variants in SOX5 have been significantly associated with multiple cardiac diseases or traits, including the higher RHR (6), electrocardiographic PR interval (7), AF (8) and LVM (9). This is the first report of a systematic assessment of the functional role of the *Drosophila* ortholog of SOX5 in a whole animal *in vivo*. These findings implicate that SOX5 may play an important role in regulating cardiac function.

We have developed a high-speed and ultrahigh-resolution OCT imaging system that enables successful characterization of structural and dynamical parameters of cardiac function in adult flies. Notably, the cardiac wall thickness is  $\sim 10$   $\mu$ m, and the differences between the two groups included in this study were  $<2$   $\mu$ m. This highlights the necessity of using a high-resolution imaging system in order to be able to distinguish these subtle differences. Moreover, as the velocity of the heart wall is relatively low, as opposed to the velocity of blood flow traditionally measured with Doppler OCT methods, imaging and analysis protocols need to be carefully designed in order to overcome the deleterious effects of phase noise and bulk sample motion. A high-speed imaging system is imperative in this respect, as extracting Doppler information from rapidly scanned cross-sectional images is more reliable and robust compared with using an M-mode image from a single transverse position. This is due to the additional structural information gained from cross-sections. Higher speed imaging systems will provide

**Table 1.** Comparison of the cardiac structural and dynamical parameters in control flies and UAS-*Sox102F*-RNAi; 24B-GAL4 flies derived from the OCT images

	Parameter (mean $\pm$ SE)	24B-GAL4/+ ( $n = 36$ )	UAS- <i>Sox102F</i> -RNAi; 24B-GAL4 ( $n = 35$ )	P-value
Structural parameters	ESDt ( $\mu\text{m}$ )	32 $\pm$ 4	19 $\pm$ 3	0.001*
	EDDt ( $\mu\text{m}$ )	64 $\pm$ 4	54 $\pm$ 3	0.02*
	ESDv ( $\mu\text{m}$ )	37 $\pm$ 4	19 $\pm$ 3	<0.0001*
	EDDv ( $\mu\text{m}$ )	71 $\pm$ 4	53 $\pm$ 4	0.0006*
	ESA ( $\mu\text{m}^2$ )	1233 $\pm$ 160	562 $\pm$ 149	0.002*
	EDA ( $\mu\text{m}^2$ )	3473 $\pm$ 300	2241 $\pm$ 265	0.002*
	Cardiac wall thickness ( $\mu\text{m}$ )	10.80 $\pm$ 0.28	12.23 $\pm$ 0.30	0.0006*
	HR (BPM)	239 $\pm$ 8	211 $\pm$ 10	0.02*
Dynamical parameters	Systolic wall velocity ( $\mu\text{m}/\text{s}$ )	877 $\pm$ 64	724 $\pm$ 33	0.02*
	Diastolic wall velocity ( $\mu\text{m}/\text{s}$ )	762 $\pm$ 41	575 $\pm$ 29	0.0002*
	Arrhythmia prevalence	15/35 (42%)	21/36 (60%)	0.1

\*Statistically significant difference,  $P < 0.05$ .

4D data sets (3D + time) in high frame rates, which will allow characterizing the velocity and other functional parameters along the entire heart tube of the fly. Important parameters such as cardiac output ( $Q$ ) can then be extracted from the 4D (3D + time) data sets for the comprehensive assessment of cardiac function.

The Wnt signal transduction has been implicated as an important event that regulates cardiac development and function (43). The Wnt signaling pathway controls  $\beta$ -catenin, which enters the nucleus, binds to DNA and triggers expression of genes (44). SOX5 acts synergistically with a stable form of  $\beta$ -catenin and increases the expression of axin2, a negative regulator of the Wnt pathway in neural tube cells (5). Consistent with previous findings, we have demonstrated that the silencing of *Sox102F* promoted the formation of wing marginal veins and a remarkably increased and disorganized level of *wg* expression in flies. These data support the contention that SOX5 negatively regulates Wnt signaling via reducing *wg* expression in addition to increasing *axin2* expression. The finding that the silencing of *Sox102F* resulted in cardiac hypertrophy accompanied with remarkably increased *wg* expression is consistent with the known role of Wnt signaling in heart formation. Down-regulation of the Wnt pathway leads to a thinner cardiac tube by gene expression profiling in *Drosophila* heart formation (45). The inhibition of *Sox102F* on the Wnt signaling may contribute to the pathogenesis that led to cardiac dysfunction in flies in which *Sox102F* was silenced.

A single-nucleotide polymorphism (SNP) rs17287293 which is located 3' to *SOX5* was significantly associated with the higher RHR in a meta-analysis of 15 GWASs (6). Epidemiologic studies have demonstrated that the higher RHR is significantly associated with increased cardiovascular disease and mortality risk independent of traditional risk factors in diverse subgroups, including healthy people in the general population (46,47), hypertensives (48) and those with established ischemic heart disease (47,49,50). A higher RHR also has been associated with poorer prognosis within subgroups of patients with cardiovascular disease (51–53). Compared with those whose RHR was consistent at <70 BPM, individuals whose rates increased from <70 to >85 BPM had a 90% higher risk of death from heart disease after 12 years of follow-up of 29 325 healthy men and women who had no known heart disease at the start of the study (50). In a 5-year follow-up, 5139 healthy middle-aged

men who showed that an increase of >3 BPM in the RHR was associated with a 19% increase in all-cause mortality (54).

In other GWASs, the SNP rs11047543 located 3' to *SOX5* was significantly associated with both the electrocardiographic PR interval (7) and AF (8). The disturbances of the PR interval is considered an intermediate phenotype for AF and an increase risk of AF, which is independently associated with an increased risk of stroke, heart failure, dementia and death. The minor allele of SNP rs11047543 was significantly associated with a decrease in AF risk (7). Furthermore, the SNP rs10743465 3' to *SOX5* was the most significantly associated with LVM in a follow-up study for LVM on chromosome 12p11 (9). An increase in LVM is one of the most important cardiac risk factors for stroke, myocardial infarction and chronic heart failure, independent of age, sex and race-ethnicity (55,56). In a landmark study, each 50 g/m increase in LVM was associated with an adjusted relative risk of cardiovascular disease of 1.49 and 1.57 in men and women, respectively (57). Moreover, diastolic dysfunction is linked to increased mortality in a range of conditions, including post-acute myocardial infarction, hypertension and chronic renal failure (58–62). Closely linked to diastolic function, alterations in cardiac wall velocities are associated with several cardiovascular disorders, mostly pronounced with hypertrophic cardiomyopathy (63–68).

An action potential is the first step in the chain of events leading to contraction in cardiac cells. The action potential stimulates  $\text{Ca}^{++}$  entry into cardiomyocytes through voltage-gated L-type  $\text{Ca}^{++}$  channels (LTCCs). Antisense oligonucleotides against *SOX5* have been shown to significantly decrease the maximum charge movement in mouse myoblast cells (69). Charge movement is regulated by LTCCs (69), and the amplitude of LTCCs was increased in hypertrophied and failing myocytes, contributing to cardiac hypertrophy (70). Moreover, the nitric oxide (NO) level is significantly correlated with the occurrence of LVM (71). *SOX5* regulated shear stress-modulated gene expression in an NO-dependent manner in endothelial cells (72), which may contribute to LVM pathogenesis. Collectively, these findings suggest that *Sox5* may regulate LTCCs and that genetic variants in *SOX5* may alter atrial action potential and atrioventricular conduction influencing risk for the higher RHR, disturbed PR interval, AF and LVM (73).

In addition to associations with cardiac diseases or traits, the SNP rs11046966 3' to *SOX5* has been associated with chronic obstructive pulmonary disease (10); the intronic SNP rs1522232 in

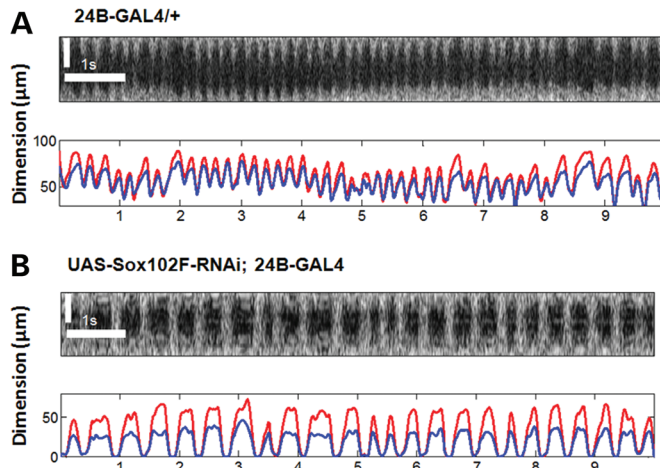


**Figure 2.** Obtaining functional information about cardiac function from structural OCT images. **(A)** A pseudo M-mode OCT image from the center of the main heart chamber (top) and the automatically generated plots for the heart dimensions (below) of a fly from the control group. Rapidly repeated cross-sectional OCT images over the clearest and largest heart chamber were performed for each fly where the single A-scan over the center of the heart chamber in each cross-sectional image is extracted to create a pseudo M-mode OCT image. The regularity of the heart beats can be visualized from the M-mode image as well as the resulting dimension plot. This particular fly has been characterized with a HR of 258 BPM, EDDt and EDDv of 80 and 108  $\mu\text{m}$ , respectively, ESDt and ESDv of 49 and 71  $\mu\text{m}$ , respectively, ESA and EDA of 2605 and 5644  $\mu\text{m}^2$ , respectively. **(B)** A pseudo M-mode OCT image (top) and the automatically generated plots for the heart dimensions (bottom) of a fly from the UAS-Sox102F-RNAi; 24B-GAL4 group. The M-mode image shows irregular beating patterns. This particular fly has been characterized with a HR of 138 BPM, EDDt and EDDv of 54 and 32  $\mu\text{m}$ , respectively, ESDt and ESDv of 1 and 1.4  $\mu\text{m}$ , respectively, ESA and EDA of 6 and 1036  $\mu\text{m}^2$ , respectively. Red lines in the dimension plots correspond to axial dimensions, whereas the blue lines correspond to transverse dimensions. Scale bars: 50  $\mu\text{m}$  in the vertical dimension; 1 s in the horizontal dimension.

SOX5 was associated with the rapid progression of AIDS (74); the other intronic SNP rs1464500 in SOX5 was associated with metabolic side effects of antipsychotic drugs, such as high-density lipoprotein levels in patients taking perphenazine (75) and triglyceride levels in subjects taking statins (76). Moreover, two missense mutations in SOX5, Gln362Pro and Glu367Gln, five amino acids apart, were identified in 2 of the 190 amyotrophic lateral sclerosis patients and not detected in 190 normal controls (77). Further studies are warranted to elucidate the functional role(s) of SOX5 in multiple human diseases or traits.

In summary, we have demonstrated that the silencing of *Sox102F* in the *Drosophila* heart results in cardiac dysfunction. Together, these data provide the first *in vivo* evidence for an important functional role for SOX5 in the heart and suggest that the alterations in SOX5 levels may contribute to the pathogenesis of multiple cardiac diseases or traits.

## MATERIALS AND METHODS

### Transgenic flies and fly culture

Fly culture and crosses were carried out according to the standard procedures. The following fly strains were used: UAS-Sox102F-RNAi from the TRIP Project at Harvard Medical

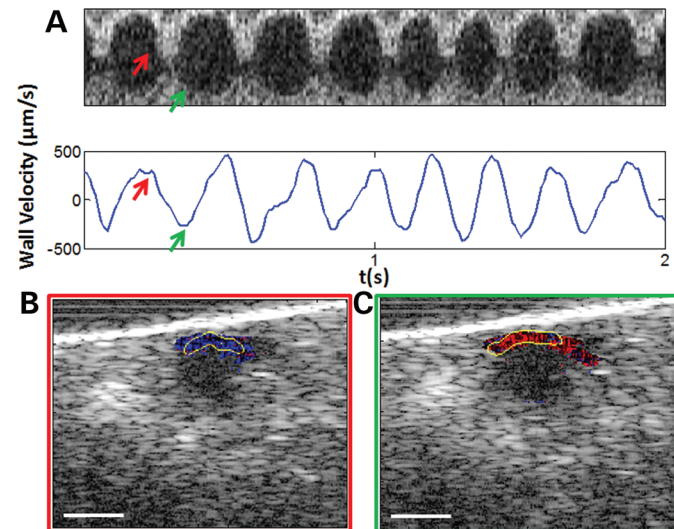


**Figure 3.** Extracting systolic and diastolic wall velocities using Doppler OCT. **(A)** A pseudo M-mode OCT image from the center of the main heart chamber (top) and the corresponding wall velocity plot extracted by Doppler analysis (bottom). A positive peak velocity is observed during the systole (an example is indicated by the red arrows), and a negative peak velocity is observed during the diastole (an example is indicated by the green arrows). A smoothing filter has been applied to the Doppler plot in order to highlight the velocity profile more clearly. **(B and C)** Cross-sectional color Doppler OCT image showing the localization of the Doppler signal at the upper portion of the heart wall during the systolic and diastolic phases. The outer boundary of the automatically segmented heart wall is shown by the yellow curve. Scale bars: 50  $\mu\text{m}$ .

School (<http://www.flrynai.org/TRIP-HOME.html>), 24B-GAL4 (38) and SD-GAL4 (42).

### Animal preparation

Flies were anesthetized in a closed container using FlyNap® (Carolina Biological Supply Company) for 2 min. FlyNap® is an established anesthetizing agent used in *Drosophila* studies, and its main constituent, triethylamine, is shown to have minimal effect on influencing fly cardiac functions (13). After anesthesia, flies were taped on a microscope cover slide by their wings with the dorsal side facing up. OCT imaging was conducted within 30 min, before the effects of anesthesia wore off in order to minimize motion artifacts.

### High-speed and ultrahigh-resolution OCT imaging system and OCT imaging for the *Drosophila* cardiac function assessment

A custom-built spectral domain OCT system was used for the study. The OCT system was optimized for high-speed and ultrahigh-resolution imaging, where a broadband superluminescent diode (Superlum, Dublin, Ireland) centered at  $\sim 850$  nm was employed to provide  $\sim 3$   $\mu\text{m}$  axial resolutions in tissue. A long working distance near infrared objective (Thorlabs, Newton, NJ, USA) was used to achieve 8  $\mu\text{m}$  resolution in the transverse dimensions. A 25 kHz line rate line-scan camera (e2v, Chelmsford, UK) was used to generate cross-sectional images at 110 frames/s with 226 axial scans per frame, which is sufficient to capture the chamber morphology at various

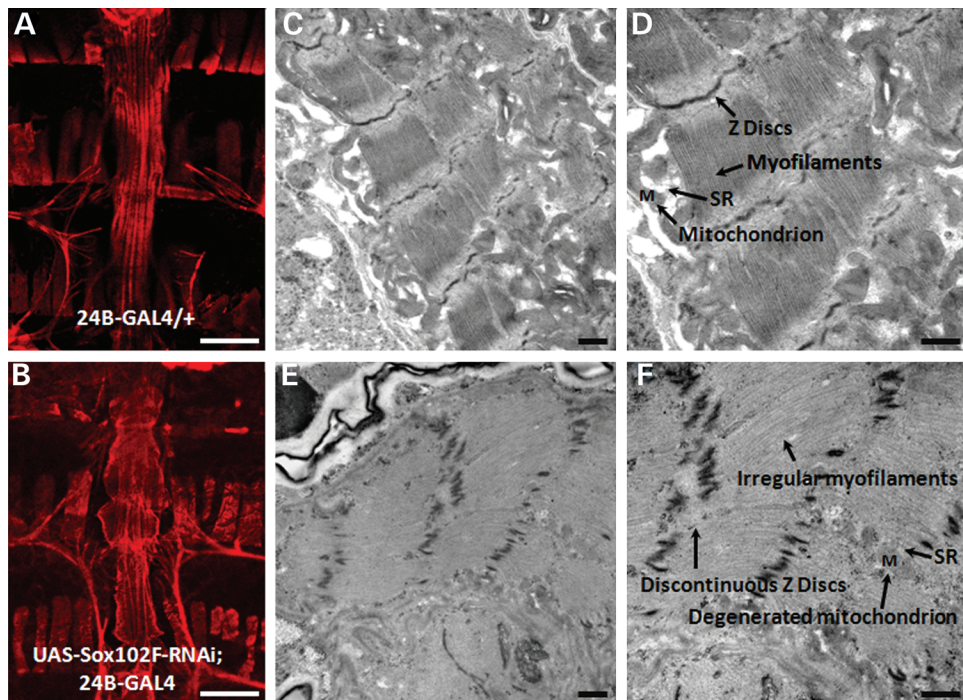


**Figure 4.** Whole heart and cardiac ultrastructure analysis. (A and B) Micrographs of the whole adult heart by F-actin immuno-fluorescent staining. (A) Control fly (24B-GAL4/+) showed a normal cardiac tube. (B) Silencing of *Sox102F* in the heart (UAS-*Sox102F*-RNAi; 24B-GAL4) resulted in an enlarged and irregular cardiac tube and loss of myofibril structure. (C–F) Ultrastructure of adult heart longitudinal sections between A1 and A3 segments by TEM. (C and D) Control fly showed normal myofibril structure. (E and F) Silencing of *Sox102F* in the heart led to irregular myofilament arrays, discontinuous Z discs, irregular and smaller SR and degenerative mitochondria. Myofilaments, Z discs, SR and mitochondrion were labeled and pointed with arrows. Magnification: (A and B) 10 $\times$ , scale bars: 100  $\mu$ m; (C and E) 20 000 $\times$ ; (D and F) 30 000 $\times$ , scale bars: 500 nm.

cardiac cycles of a beating fly heart. The imaging speed and the transverse imaging resolution were improved by a factor of  $\sim 2$ , and the axial resolution is improved by more than a factor of 3 compared with the OCT system used in our previous studies on *Drosophila* (36). Dynamical and structural parameters including HR, ESDv, ESDt, EDDv, EDDt, ESA, EDA, wall thickness and systolic and diastolic wall velocities of the heart wall were extracted from cross-sectional images obtained from the heart chamber  $\sim 50$   $\mu$ m away from the chest. This cross-sectional imaging plane was selected for analysis as it consistently presents the clearest and largest heart chamber in all the flies. Each cross-sectional imaging session was acquired continuously for 10 s and repeated three times in order to capture multiple cardiac cycles for accurate analysis. Post-processing of the image data was performed with the custom-written MATLAB (Mathworks, Natick, MA, USA) code. The prevalence of arrhythmia in each fly group (%) was quantitatively analyzed via identifying the irregular heartbeat rhythm in the dimension plots.

Since the *Drosophila* hemolymph is essentially transparent due to lack of red blood cells, obtaining flow information from the hemolymph is not possible without using extrinsic contrast agents. However, it is possible to extract Doppler OCT information from the heart wall as demonstrated in previous studies (35,37). Doppler analysis of the cardiac wall relied on an established method in the OCT literature, which requires oversampling in the spatial dimension and extracting motion information by finding the phase difference between two successive A-scans and correcting the calculated phase for bulk motion effects (78,79). We were able to extract systolic and diastolic

cardiac wall velocity profiles from the flies using Doppler OCT. The upper portion of the heart wall was automatically segmented in order to calculate velocity from the region of the wall that has movement in the vertical direction, as the Doppler analysis method employed in this study can only measure velocity in parallel to the scanning beam. From the resulting M-mode Doppler velocity plots, systolic and diastolic wall velocities were calculated by finding the mean of positive and negative peak velocity values, respectively.

#### ***Drosophila* heart structural analysis by F-actin immunostaining microscopy and TEM**

Hearts from 30-day-old control or silencing of *Sox102F* flies were dissected for whole heart and cardiac ultrastructure analyses. Fluorescent labeling of the whole adult heart tube with F-actin and imaging were done as described previously (80). In brief, 15 hearts from control or silencing of *Sox102F* flies were dissected in oxygenated hemolymph and fixed with 4% formaldehyde. The sarcomeric F-actin was stained with Alexa-Fluor® 594 phalloidin (red, Life Technologies, Grand Island, NY, USA) and imaged with a Zeiss confocal microscope. For TEM, 15 hearts from control or silencing of *Sox102F* flies were fixed, embedded, sectioned, examined and imaged as described previously (81). In brief, tissues were fixed in 2.0% glutaraldehyde in 0.1 M sodium cacodylate buffer, pH 7.4 (Electron Microscopy Sciences, Hatfield, PA, USA) overnight at 4°C. They were rinsed in buffer, post-fixed in 1.0% osmium tetroxide in cacodylate buffer for 1 h at room temperature, rinsed in buffer

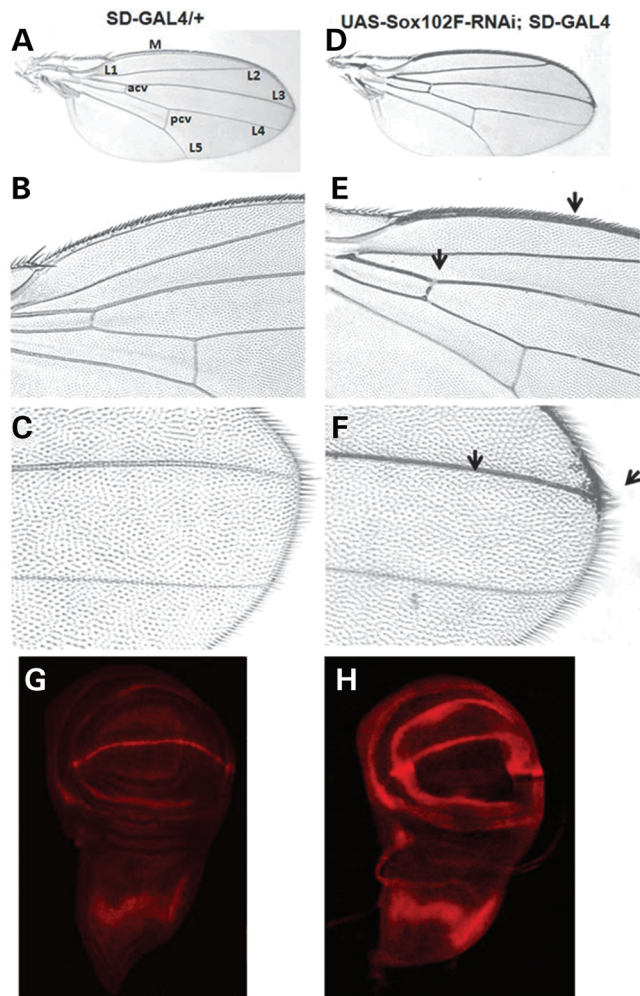


**Figure 5.** Silencing of *Sox102F* in the wing resulted in wing vein phenotypes and altered *wg* expression in wing disc. (A–C) Control fly with heterozygous *SD-GAL4* driver alone (*SD-GAL4/+*) showed normal wing structure. (D–F) Silencing of *Sox102F* in the wing (UAS-*Sox102F-RNAi*; *SD-GAL4*) led to a significant increase in the L2, L3 and wing marginal veins; in particular, extra veins were formed in the distal part of L3 vein (arrows). (G) In control flies, *wg* was expressed as a broad strip in the notum, a thinner strip in the prospective wing margin-D/V boundary and a strip encircling the prospective wing blade. (H) In flies in which *Sox102F* was silenced, there were increased *wg* expression level and disorganized *wg* expression pattern, forming extra strips in the prospective wing blade region.

and dehydrated through a graded series of ethanol to 100%. They were then infiltrated with Epon resin (Ted Pella, Redding, CA, USA) in a 1:1 solution of Epon:ethanol. The following day they were placed in fresh Epon for several hours and then embedded in Epon overnight at 60°C. Thin sections were cut on a Leica EM UC7 ultramicrotome, collected on formvar-coated grids, stained with uranyl acetate and lead citrate and examined in a JEOL JEM 1011 transmission electron microscope at 80 kV. Images were collected using an AMT digital imaging system (Advanced Microscopy Techniques, Danvers, MA, USA).

#### Analysis of the wing phenotype and immunostaining for *wg* expression

Wings from adult flies were dissected in isopropanol and mounted in Canada Balsam mounting medium. A total of 30

third instar wing discs were dissected, fixed, blocked and probed with primary and secondary antibodies accordingly. The following antibodies were used: mouse anti-*wg* antibody (1:1000, Developmental Studies Hybridoma Bank, Iowa City, IA, USA) and the secondary anti-mouse Alexa 546 (1:200, Life Technologies).

#### cDNA synthesis and real-time RT–PCR

The cDNAs used for real-time RT–PCR were synthesized from total RNA isolated from the heart muscle of 30-day-old adult *Drosophila*. The cDNA was synthesized using SUPERSCRIPT Preamplification System for first-strand cDNA synthesis (Life Technologies). Real-time RT–PCR quantification with *Sox102F* or *dActin*-specific sense and antisense primers was done on an iCycler (BIO-RAD, Hercules, CA, USA) using SYBR Green PCR Core Reagents (Qiagen, Germantown, MD, USA) according to the manufacturer's instructions. The sequences of primers are: *Sox102F* 5'-TGGTGGCTCA GGAAGTCTCT, 3'-AACTGCTGAGGGGGTGTATG; RT–PCR product size 171 bp; *Actin5C* 5'-TACCCCATGAGCA CGGTAT, 3'-GGTCATCTTCTCACGGTTGG; RT–PCR product size 156 bp. The house-keeping gene *dActin* was used as an internal control and was co-amplified under the same PCR conditions. All standards and unknown samples were run in triplicates per reaction. The fluorescence intensity was calculated using iCycler software version 3.1. The expressions of *Sox102F* were given as a relative number of copies (%) of mRNA molecules, as calibrated by co-amplification of *dActin*.

#### Statistical analysis of cardiac function

A custom MATLAB (Mathworks) script was used to automatically segment the fly heart chamber from cross-sectional OCT images and extract functional and structural parameters described previously. Average values for these parameters were calculated from the measurement of multiple cardiac cycles and repeated imaging sessions. The mean  $\pm$  SE of each parameter was reported for each fly group.

The Student's *t*-test was performed to statistically compare the difference between the UAS-*Sox102F-RNAi*; 24B-GAL4 group and the aged matched 24B-GAL4/+ control group and  $P < 0.05$  was defined as statistically significant. Irregular heartbeat rhythm was identified if it occurred during imaging and the prevalence of cardiac arrhythmia was statistically compared between the two groups using a two-proportion *z*-test.

*Conflict of Interest statement.* None declared.

#### FUNDING

This work was supported by the Cure Alzheimer's Fund to R.E.T., the National Institute of Health (R01AG014713 and R01MH60009 to R.E.T.; R01CA75289 and R01HL095717 to J.G.F.; R00EB010071 to C.Z.; R03AR063271 to A.L.), the Air Force Office of Scientific Research (FA9550-07-1-0014 to J.G.F.) and a Massachusetts General Hospital ECOR Award to A.L. The Microscopy Core Facility at the MGH Program in Membrane Biology receives support from the Boston

Area Diabetes and Endocrinology Research Center (DK 57521) and the Center for the Study of Inflammatory Bowel Disease (DK 43351).

## REFERENCES

- Remenyi, A., Lins, K., Nissen, L.J., Reinbold, R., Scholer, H.R. and Wilmanns, M. (2003) Crystal structure of a POU/HMG/DNA ternary complex suggests differential assembly of Oct4 and Sox2 on two enhancers. *Genes Dev.*, **17**, 2048–2059.
- Wunderle, V.M., Critcher, R., Ashworth, A. and Goodfellow, P.N. (1996) Cloning and characterization of SOX5, a new member of the human SOX gene family. *Genomics*, **36**, 354–358.
- Smits, P., Li, P., Mandel, J., Zhang, Z., Deng, J.M., Behringer, R.R., de Crombrugge, B. and Lefebvre, V. (2001) The transcription factors L-Sox5 and Sox6 are essential for cartilage formation. *Dev. Cell*, **1**, 277–290.
- Shim, S., Kwan, K.Y., Li, M., Lefebvre, V. and Sestan, N. (2012) Cis-regulatory control of corticospinal system development and evolution. *Nature*, **486**, 74–79.
- Martinez-Morales, P.L., Quiroga, A.C., Barbas, J.A. and Morales, A.V. (2010) SOX5 controls cell cycle progression in neural progenitors by interfering with the WNT-beta-catenin pathway. *EMBO Rep.*, **11**, 466–472.
- Eijgelsheim, M., Newton-Cheh, C., Sotoodehnia, N., de Bakker, P.I., Muller, M., Morrison, A.C., Smith, A.V., Isaacs, A., Sanna, S., Dorr, M. et al. (2010) Genome-wide association analysis identifies multiple loci related to resting heart rate. *Hum. Mol. Genet.*, **19**, 3885–3894.
- Pfeufer, A., van Noord, C., Marcante, K.D., Arking, D.E., Larson, M.G., Smith, A.V., Tarasov, K.V., Muller, M., Sotoodehnia, N., Sinner, M.F. et al. (2010) Genome-wide association study of PR interval. *Nat. Genet.*, **42**, 153–159.
- Olesen, M.S., Holst, A.G., Jabbari, J., Nielsen, J.B., Christoffersen, I.E., Sajadieh, A., Haunso, S. and Svendsen, J.H. (2012) Genetic loci on chromosomes 4q25, 7p31, and 12p12 are associated with onset of lone atrial fibrillation before the age of 40 years. *Can. J. Cardiol.*, **28**, 191–195.
- Della-Morte, D., Beecham, A., Rundek, T., Wang, L., McClendon, M.S., Slifer, S., Blanton, S.H., Di Tullio, M.R. and Sacco, R.L. (2011) A follow-up study for left ventricular mass on chromosome 12p11 identifies potential candidate genes. *BMC Med. Genet.*, **12**, 100.
- Hersh, C.P., Silverman, E.K., Gascon, J., Bhattacharya, S., Klanderman, B.J., Litonjua, A.A., Lefebvre, V., Sparrow, D., Reilly, J.J., Anderson, W.H. et al. (2011) SOX5 is a candidate gene for chronic obstructive pulmonary disease susceptibility and is necessary for lung development. *Am. J. Respir. Crit. Care Med.*, **183**, 1482–1489.
- Ocorr, K., Reeves, N.L., Wessells, R.J., Fink, M., Chen, H.S., Akasaki, T., Yasuda, S., Metzger, J.M., Giles, W., Posakony, J.W. et al. (2007) KCNQ potassium channel mutations cause cardiac arrhythmias in *Drosophila* that mimic the effects of aging. *Proc. Natl Acad. Sci. USA*, **104**, 3943–3948.
- Vigoreaux, J.O. (2001) Genetics of the *Drosophila* flight muscle myofibril: a window into the biology of complex systems. *Bioessays*, **23**, 1047–1063.
- Paterno, G., Vignola, C., Bartsch, D.U., Omens, J.H., McCulloch, A.D. and Reed, J.C. (2001) Age-associated cardiac dysfunction in *Drosophila melanogaster*. *Circ. Res.*, **88**, 1053–1058.
- Curtis, N.J., Ringo, J.M. and Dowse, H.B. (1999) Morphology of the pupal heart, adult heart, and associated tissues in the fruit fly, *Drosophila melanogaster*. *J. Morphol.*, **240**, 225–235.
- Nishimura, M., Ocorr, K., Bodmer, R. and Cartry, J. (2011) *Drosophila* as a model to study cardiac aging. *Exp. Gerontol.*, **46**, 326–330.
- Huang, D., Swanson, E.A., Lin, C.P., Schuman, J.S., Stinson, W.G., Chang, W., Hee, M.R., Flotte, T., Gregory, K., Puliafito, C.A. et al. (1991) Optical coherence tomography. *Science*, **254**, 1178–1181.
- Drexler, W., Morgner, U., Ghanta, R.K., Kärtner, F.X., Schuman, J.S. and Fujimoto, J.G. (2001) Ultrahigh-resolution ophthalmic optical coherence tomography. *Nat. Med.*, **7**, 502–507.
- Sakata, L.M., DeLeon-Ortega, J., Sakata, V. and Girkin, C.A. (2009) Optical coherence tomography of the retina and optic nerve - a review. *Clin. Exp. Ophthalmol.*, **37**, 90–99.
- Geitzenauer, W., Hitzenberger, C.K. and Schmidt-Erfurth, U.M. (2011) Retinal optical coherence tomography: past, present and future perspectives. *Br. J. Ophthalmol.*, **95**, 171–177.
- Tearney, G.J., Brezinski, M.E., Bouma, B.E., Boppart, S.A., Pitvis, C., Southern, J.F. and Fujimoto, J.G. (1997) *In vivo* endoscopic optical biopsy with optical coherence tomography. *Science*, **276**, 2037–2039.
- Bouma, B.E., Tearney, G.J., Compton, C.C. and Nishioka, N.S. (2000) High-resolution imaging of the human esophagus and stomach *in vivo* using optical coherence tomography. *Gastrointest. Endosc.*, **51**, 467–474.
- Sivak, M.V., Kobayashi, K., Izatt, J.A., Rollins, A.M., Ung-runyawee, R., Chak, A., Wong, R.C.K., Isenberg, G.A. and Willis, J. (2000) High-resolution endoscopic imaging of the GI tract using optical coherence tomography. *Gastrointest. Endosc.*, **51**, 474–479.
- Suter, M.J., Jillella, P.A., Vakoc, B.J., Halpern, E.F., Mino-Kenudson, M., Lauwers, G.Y., Bouma, B.E., Nishioka, N.S. and Tearney, G.J. (2010) Image-guided biopsy in the esophagus through comprehensive optical frequency domain imaging and laser marking: a study in living swine. *Gastrointest. Endosc.*, **71**, 346–353.
- Li, X.D., Boppart, S.A., Van Dam, J., Mashimo, H., Mutinga, M., Drexler, W., Klein, M., Pitriss, C., Krinsky, M.L., Brezinski, M.E. et al. (2000) Optical coherence tomography: advanced technology for the endoscopic imaging of Barrett's esophagus. *Endoscopy*, **32**, 921–930.
- Hatta, W., Uno, K., Koike, T., Yokosawa, S., Iijima, K., Imatani, A. and Shimosegawa, T. (2010) Optical coherence tomography for the staging of tumor infiltration in superficial esophageal squamous cell carcinoma. *Gastrointest. Endosc.*, **71**, 899–906.
- Zhou, C., Tsai, T.H., Lee, H.C., Kirtane, T., Figueiredo, M., Tao, Y.K.K., Ahsen, O.O., Adler, D.C., Schmitt, J.M., Huang, Q. et al. (2012) Characterization of buried glands before and after radiofrequency ablation by using 3-dimensional optical coherence tomography (with videos). *Gastrointest. Endosc.*, **76**, 32–40.
- Tearney, G.J., Brezinski, M.E., Southern, J.F., Bouma, B.E., Boppart, S.A. and Fujimoto, J.G. (1997) Optical biopsy in human gastrointestinal tissue using optical coherence tomography. *Am. J. Gastroenterol.*, **92**, 1800–1804.
- Barlis, P., van Soest, G., Serruys, P.W. and Regar, E. (2009) Intracoronary optical coherence tomography and the evaluation of stents. *Exp. Rev. Med. Devices*, **6**, 157–167.
- Bezerra, H.G., Costa, M.A., Guagliumi, G., Rollins, A.M. and Simon, D.I. (2009) Intracoronary optical coherence tomography: a comprehensive review clinical and research applications. *JACC Cardiovasc. Interv.*, **2**, 1035–1046.
- Jang, I.K., Bouma, B.E., Kang, D.H., Park, S.J., Park, S.W., Seung, K.B., Choi, K.B., Shishkov, M., Schlendorf, K., Pomerantsev, E. et al. (2002) Visualization of coronary atherosclerotic plaques in patients using optical coherence tomography: comparison with intravascular ultrasound. *J. Am. Coll. Cardiol.*, **39**, 604–609.
- Gutierrez-Chico, J.L., Alegria-Barbero, E., Teijeiro-Mestre, R., Chan, P.H., Tsujioka, H., de Silva, R., Viceconte, N., Lindsay, A., Patterson, T., Foin, N. et al. (2012) Optical coherence tomography: from research to practice. *Eur. Heart J. Cardiovasc. Imaging*, **13**, 370–384.
- Wolf, M.J., Amrein, H., Izatt, J.A., Choma, M.A., Reedy, M.C. and Rockman, H.A. (2006) *Drosophila* as a model for the identification of genes causing adult human heart disease. *Proc. Natl Acad. Sci. USA*, **103**, 1394–1399.
- Choma, M.A., Izatt, S.D., Wessells, R.J., Bodmer, R. and Izatt, J.A. (2006) Images in cardiovascular medicine: *in vivo* imaging of the adult *Drosophila melanogaster* heart with real-time optical coherence tomography. *Circulation*, **114**, e35–e36.
- Allikian, M.J., Bhabha, G., Dosopy, P., Heydemann, A., Ryder, P., Earley, J.U., Wolf, M.J., Rockman, H.A. and McNally, E.M. (2007) Reduced life span with heart and muscle dysfunction in *Drosophila sarcoglycan* mutants. *Hum. Mol. Genet.*, **16**, 2933–2943.
- Choma, M.A., Suter, M.J., Vakoc, B.J., Bouma, B.E. and Tearney, G.J. (2010) Heart wall velocimetry and exogenous contrast-based cardiac flow imaging in *Drosophila melanogaster* using Doppler optical coherence tomography. *J. Biomed. Optics*, **15**, 056020.
- Li, A., Zhou, C., Moore, J., Zhang, P., Tsai, T.H., Lee, H.C., Romano, D.M., McKee, M.L., Schoenfeld, D.A., Serra, M.J. et al. (2011) Changes in the expression of the Alzheimer's disease-associated presenilin gene in *Drosophila* heart leads to cardiac dysfunction. *Curr. Alzheimer Res.*, **8**, 313–322.
- Choma, M.A., Suter, M.J., Vakoc, B.J., Bouma, B.E. and Tearney, G.J. (2011) Physiological homology between *Drosophila melanogaster* and vertebrate cardiovascular systems. *Dis. Models Mech.*, **4**, 411–420.
- Brand, A.H. and Perrimon, N. (1993) Targeted gene expression as a means of altering cell fates and generating dominant phenotypes. *Development*, **118**, 401–415.
- Fischer, J.A., Giniger, E., Maniatis, T. and Ptashne, M. (1988) Gal4 activates transcription in *Drosophila*. *Nature*, **332**, 853–856.

40. Zikova, M., Da Ponte, J.P., Dastugue, B. and Jagla, K. (2003) Patterning of the cardiac outflow region in *Drosophila*. *Proc. Natl Acad. Sci. USA*, **100**, 12189–12194.
41. Sturtevant, M.A. and Bier, E. (1995) Analysis of the genetic hierarchy guiding wing vein development in *Drosophila*. *Development*, **121**, 785–801.
42. Paumard-Rigal, S., Zider, A., Vaudin, P. and Silber, J. (1998) Specific interactions between vestigial and scalloped are required to promote wing tissue proliferation in *Drosophila melanogaster*. *Dev. Genes. Evol.*, **208**, 440–446.
43. Eisenberg, L.M. and Eisenberg, C.A. (2006) Wnt signal transduction and the formation of the myocardium. *Dev. Biol.*, **293**, 305–315.
44. Liebner, S., Cattelino, A., Gallini, R., Rudini, N., Iurlaro, M., Piccolo, S. and Dejana, E. (2004) Beta-catenin is required for endothelial-mesenchymal transformation during heart cushion development in the mouse. *J. Cell. Biol.*, **166**, 359–367.
45. Zeitouni, B., Senatore, S., Severac, D., Aknin, C., Semeriva, M. and Perrin, L. (2007) Signalling pathways involved in adult heart formation revealed by gene expression profiling in *Drosophila*. *PLoS Genet.*, **3**, 1907–1921.
46. Cooney, M.T., Virtainen, E., Laatikainen, T., Juolevi, A., Dudina, A. and Graham, I.M. (2009) Elevated resting heart rate is an independent risk factor for cardiovascular disease in healthy men and women. *Am. Heart J.*, **159**, 612–619 e613.
47. Kannel, W.B., Kannel, C., Paffenbarger, R.S. Jr and Cupples, L.A. (1987) Heart rate and cardiovascular mortality: the Framingham study. *Am. Heart J.*, **113**, 1489–1494.
48. Benetos, A., Rudnicki, A., Thomas, F., Safar, M. and Guize, L. (1999) Influence of heart rate on mortality in a French population: role of age, gender, and blood pressure. *Hypertension*, **33**, 44–52.
49. Woodward, M., Webster, R., Murakami, Y., Barzi, F., Lam, T.H., Fang, X., Suh, I., Batty, G.D., Huxley, R. and Rodgers, A. (2012) The association between resting heart rate, cardiovascular disease and mortality: evidence from 112,680 men and women in 12 cohorts. *Eur. J. Prev. Cardiol.* doi:10.1177/2047487312452501.
50. Nauman, J., Janszky, I., Vatten, L.J. and Wisloff, U. (2011) Temporal changes in resting heart rate and deaths from ischemic heart disease. *JAMA*, **306**, 2579–2587.
51. Fox, K., Ford, I., Steg, P.G., Tendera, M., Robertson, M. and Ferrari, R. (2008) Heart rate as a prognostic risk factor in patients with coronary artery disease and left-ventricular systolic dysfunction (BEAUTIFUL): a subgroup analysis of a randomised controlled trial. *Lancet*, **372**, 817–821.
52. Fox, K. and Steg, P.G. (2008) Elevated heart rate proven to increase coronary events. *Cardiovasc. J. Afr.*, **19**, 276–278.
53. Diaz, A., Bourassa, M.G., Guertin, M.C. and Tardif, J.C. (2005) Long-term prognostic value of resting heart rate in patients with suspected or proven coronary artery disease. *Eur. Heart J.*, **26**, 967–974.
54. Jouven, X., Empana, J.P., Escolano, S., Buyck, J.F., Tafflet, M., Desnos, M. and Ducimetiere, P. (2009) Relation of heart rate at rest and long-term (>20 years) death rate in initially healthy middle-aged men. *Am. J. Cardiol.*, **103**, 279–283.
55. Gosse, P. and Dalloccchio, M. (1993) Left ventricular hypertrophy: epidemiological prognosis and associated critical factors. *Eur. Heart J.*, **14** (Suppl. D), 16–21.
56. Haider, A.W., Larson, M.G., Benjamin, E.J. and Levy, D. (1998) Increased left ventricular mass and hypertrophy are associated with increased risk for sudden death. *J. Am. Coll. Cardiol.*, **32**, 1454–1459.
57. Levy, D., Garrison, R.J., Savage, D.D., Kannel, W.B. and Castelli, W.P. (1990) Prognostic implications of echocardiographically determined left ventricular mass in the Framingham Heart Study. *N. Engl. J. Med.*, **322**, 1561–1566.
58. Moller, J.E., Egstrup, K., Kober, L., Poulsen, S.H., Nyvad, O. and Torp-Pedersen, C. (2003) Prognostic importance of systolic and diastolic function after acute myocardial infarction. *Am. Heart J.*, **145**, 147–153.
59. Hillis, G.S., Moller, J.E., Pellikka, P.A., Gersh, B.J., Wright, R.S., Ommen, S.R., Reeder, G.S. and Oh, J.K. (2004) Noninvasive estimation of left ventricular filling pressure by E/e' is a powerful predictor of survival after acute myocardial infarction. *J. Am. Coll. Cardiol.*, **43**, 360–367.
60. Wang, M., Yip, G.W., Wang, A.Y., Zhang, Y., Ho, P.Y., Tse, M.K., Yu, C.M. and Sanderson, J.E. (2005) Tissue Doppler imaging provides incremental prognostic value in patients with systemic hypertension and left ventricular hypertrophy. *J. Hypertens.*, **23**, 183–191.
61. Sharma, R., Pellerin, D., Gaze, D.C., Mehta, R.L., Gregson, H., Streather, C.P., Collinson, P.O. and Brecker, S.J. (2006) Mitral peak Doppler E-wave to peak mitral annulus velocity ratio is an accurate estimate of left ventricular filling pressure and predicts mortality in end-stage renal disease. *J. Am. Soc. Echocardiogr.*, **19**, 266–273.
62. Nagueh, S.F., Appleton, C.P., Gillebert, T.C., Marino, P.N., Oh, J.K., Smiseth, O.A., Waggoner, A.D., Flachskampf, F.A., Pellikka, P.A. and Evangelista, A. (2009) Recommendations for the evaluation of left ventricular diastolic function by echocardiography. *J. Am. Soc. Echocardiogr.*, **22**, 107–133.
63. Matsumura, Y., Elliott, P.M., Virdee, M.S., Sorajja, P., Doi, Y. and McKenna, W.J. (2002) Left ventricular diastolic function assessed using Doppler tissue imaging in patients with hypertrophic cardiomyopathy: relation to symptoms and exercise capacity. *Heart*, **87**, 247–251.
64. Eckberg, D.L., Gault, J.H., Bouchard, R.L., Karliner, J.S. and Ross, J. (1973) Mechanics of left ventricular contraction in chronic severe mitral regurgitation. *Circulation*, **47**, 1252–1259.
65. Kovick, R.B., Fogelman, A.M., Abbasi, A.S., Peter, J.B. and Pearce, M.L. (1975) Echocardiographic evaluation of posterior left-ventricular wall motion in muscular-dystrophy. *Circulation*, **52**, 447–454.
66. Chikamori, T., Dickie, S., Poloniecki, J.D., Myers, M.J., Lavender, J.P. and McKenna, W.J. (1990) Prognostic-significance of radionuclide-assessed diastolic function in hypertrophic cardiomyopathy. *Am. J. Cardiol.*, **65**, 478–482.
67. Pak, P.H., Maughan, W.L., Baughman, K.L. and Kass, D.A. (1996) Marked discordance between dynamic and passive diastolic pressure-volume relations in idiopathic hypertrophic cardiomyopathy. *Circulation*, **94**, 52–60.
68. Galetta, F., Franzoni, F. and Santoro, G. (2004) Left ventricular diastolic function assessed using tissue Doppler imaging in elderly athletes. *Int. J. Cardiol.*, **94**, 339–340.
69. Zheng, Z., Wang, Z.M. and Delbono, O. (2002) Charge movement and transcription regulation of L-type calcium channel alpha(1S) in skeletal muscle cells. *J. Physiol.*, **540**, 397–409.
70. Benitah, J.P., Alvarez, J.L. and Gomez, A.M. (2010) L-type Ca(2+) current in ventricular cardiomyocytes. *J. Mol. Cell. Cardiol.*, **48**, 26–36.
71. Hua, L., Li, C., Xia, D., Qu, P., Li, Z., Zhang, W. and Feng, X. (2000) Relationship between hypertensive left ventricular hypertrophy and levels of endothelin and nitric oxide. *Hypertens. Res.*, **23**, 377–380.
72. Braam, B., de Roos, R., Bluyssen, H., Kemmeren, P., Holstege, F., Joles, J.A. and Koomans, H. (2005) Nitric oxide-dependent and nitric oxide-independent transcriptional responses to high shear stress in endothelial cells. *Hypertension*, **45**, 672–680.
73. Olsson, S.B., Cotoi, S. and Varanauskas, E. (1971) Monophasic action potential and sinus rhythm stability after conversion of atrial fibrillation. *Acta Med. Scand.*, **190**, 381–387.
74. Le Clerc, S., Limou, S., Coulonges, C., Carpentier, W., Dina, C., Taing, L., Delaneau, O., Labib, T., Sladek, R., Deveau, C. et al. (2009) Genomewide association study of a rapid progression cohort identifies new susceptibility alleles for AIDS (ANRS Genomewide Association Study 03). *J. Infect. Dis.*, **200**, 1194–1201.
75. Adkins, D.E., Aberg, K., McClay, J.L., Bukszar, J., Zhao, Z., Jia, P., Stroup, T.S., Perkins, D., McEvoy, J.P., Lieberman, J.A. et al. (2011) Genomewide pharmacogenomic study of metabolic side effects to antipsychotic drugs. *Mol. Psychiatry*, **16**, 321–332.
76. Barber, M.J., Mangravite, L.M., Hyde, C.L., Chasman, D.I., Smith, J.D., McCarty, C.A., Li, X., Wilke, R.A., Rieder, M.J., Williams, P.T. et al. (2010) Genome-wide association of lipid-lowering response to statins in combined study populations. *PLoS One*, **5**, e9763.
77. Daoud, H., Valdmanis, P.N., Gros-Louis, F., Belzil, V., Spiegelman, D., Henrion, E., Diallo, O., Desjarlais, A., Gauthier, J., Camu, W. et al. (2011) Resequencing of 29 candidate genes in patients with familial and sporadic amyotrophic lateral sclerosis. *Arch. Neurol.*, **68**, 587–593.
78. White, B., Pierce, M., Nassif, N., Cense, B., Park, B., Tearney, G., Bouma, B., Chen, T. and de Boer, J. (2003) *In vivo* dynamic human retinal blood flow imaging using ultra-high-speed spectral domain optical coherence tomography. *Optics Express*, **11**, 3490–3497.
79. Leitgeb, R., Schmetterer, L., Drexler, W., Fercher, A., Zawadzki, R. and Bajraszewski, T. (2003) Real-time assessment of retinal blood flow with ultrafast acquisition by color Doppler Fourier domain optical coherence tomography. *Optics Express*, **11**, 3116–3121.
80. Alayari, N.N., Vogler, G., Taghli-Lamalle, O., Ocorr, K., Bodmer, R. and Cammarato, A. (2009) Fluorescent labeling of *Drosophila* heart structures. *J. Vis. Exp.*, **32**, e1423.
81. Sullivan William, M.A. and Scott Hawley, R. (2000) *Drosophila Protocols*. Cold Spring Harbor Laboratory Press, Woodbury, NY, 245 pp.